Extraction of lifetime distributions from fluorescence decays with application to DNA-base analogues

Post-print of peer-reviewed article published by the Royal Society of Chemistry.
Published article available at: http://dx.doi.org/10.1039/C0CP01779E

Cite as:
Fogarty, A. C., Jones, A. C., & Camp, P. J. (2011). Extraction of lifetime distributions from fluorescence decays with application to DNA-base analogues. *Physical Chemistry Chemical Physics,* 13(9), 3819-3830.

Manuscript received: 11/09/2010; Accepted: 25/11/2010; Article published: 07/01/2011

Extraction of lifetime distributions from fluorescence decays with application to DNA-base analogues**

A.C. Fogarty, A.C. Jones and P.J. Camp*

[1]EaStCHEM, School of Chemistry, Joseph Black Building, University of Edinburgh, West Mains Road, Edinburgh, EH9 3JJ, UK.

[*]Corresponding author; e-mail: philip.camp@ed.ac.uk

[**]The authors are grateful to Xiaohua Wu and Mathieu Bennet for providing experimental decay data. This research was supported by the School of Chemistry at the University of Edinburgh.

Graphical abstract:

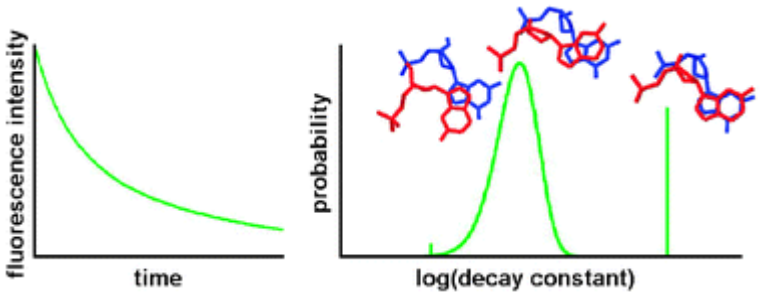

Keywords:
time-resolved fluorescence; resonance energy-transfer; maximum-entropy method; active-site; acceptor distribution; charge-transport; excited-state; 77 k; 2-aminopurine; dynamics

Abstract

Several important aspects of fluorescence decay analysis are addressed and tested against new experimental measurements. A simulated-annealing method is described for deconvoluting the instrument response function from a measured fluorescence decay to yield the true decay, which is more convenient for subsequent fitting. The method is shown to perform well against the conventional approach, which is to fit a convoluted fitting function to the experimentally measured decay. The simulated annealing approach is also successfully applied to the determination of an instrument response function using a known true fluorescence decay (for rhodamine 6G). The analysis of true fluorescence decays is considered critically, focusing specifically on how a distribution of decay constants can be incorporated in to a fit. Various fitting functions are applied to the true fluorescence decays of 2-aminopurine in water–dioxane mixtures, in a dinucleotide, and in DNA duplexes. It is shown how a suitable combination of exponential decays and non-exponential decays (based on a Γ distribution of decay constants) can provide fits of equal quality to the conventional multi-exponential fits used in the majority of previous studies, but with fewer fitting parameters. Crucially, the new approach yields decay-constant distributions that are physically more meaningful than those corresponding to the conventional multi-exponential fit. The methods presented here should find wider application, for example to the analysis of transient-current or optical decays and in Förster resonance energy transfer (FRET).

1. Introduction

Fluorescence decay (FD) data are routinely employed in the study of molecular conformations and solvation environments. A key stage in the analysis of FD data is the extraction of a lifetime, or distribution of lifetimes, associated with a particular fluorophore. In some cases, FDs can be fitted with a single exponential corresponding to a discrete lifetime or a narrow distribution of lifetimes. In more complex situations, such as those where fluorophores can adopt a variety of conformations or where they sample a range of solvation environments, the most common approach is to fit a sum of exponentials (typically up to about four). In the most naïve interpretation of the fitting parameters, the number of discrete lifetimes might indicate the number of possible conformations and/or solvation environments accessible to the fluorophore. This method has been shown to be inadequate in many situations.[1–5] Indeed, there are many complex systems which could hardly be expected to exhibit simple FDs arising from a small number of discrete fluorophore environments or conformations. Examples include fluorophores that relax electronically by energy transfer to multiple acceptors[6] and fluorophores that are adsorbed on to surfaces.[7]

It is not hard to see that a multi-exponential fit may conceal some useful information contained within the FD. For instance, a fluorophore may sample two broadly distinct conformations but experience significant fluctuations. In this case, the true distribution of lifetimes may not be determined accurately as a simple superposition of a few discrete lifetimes. In the common multi-exponential model, more and more terms have to be added in order to provide the required flexibility to fit the FD data; it is rarely true, though, that the large number of fitted lifetimes corresponds to the number of distinct fluorophore conformations. Clearly, these sums are aiming to mimic the true lifetime distribution, or at least, some of its moments. Improvements on the fitted multi-exponential model have been proposed. For example, lifetime distributions can be derived from known kinetics and structural dynamics.[7] Lifetime distributions can also be modelled with normal or log-normal probability distributions[2,6,8–10] and other functions such as the Lorentzian.[11]

Significant efforts have been made to develop methods for determining the distribution of lifetimes without having to specify in advance the number of distinct conformational manifolds (corresponding to the number of peaks in the lifetime distribution). Examples include the exponential series method[3,4,12] and the maximum entropy method.[4,13,14] In practice, however, these methods are too unconstrained to give reliable and unequivocal results in all situations. On the one hand, then, a degree of physical intuition is required to constrain the broad features of the lifetime distribution. On the other hand, there has to be sufficient flexibility in the model distribution to provide satisfactory fits to experimental FDs.

In this work, the FDs of some important fluorophores are analysed in order to establish a reliable protocol for extracting the likely number of peaks in the lifetime distribution and hence the likely number of distinct fluorophore conformations. This is achieved by comparing critically the results from multi-exponential fits (found in almost all current FD analysis software) and those obtained using new model distributions for the corresponding decay constant based on combinations of δ functions and Γ distributions.[15] The test systems under investigation are all based on DNA. The four natural bases are not fluorescent, but fluorescent analogues can be synthesised with similar molecular structures. Specifically, 2-aminopurine (2AP) is an analogue of adenine. (It can also be used as an analogue of guanine or cytosine.[16]) 2AP is a useful probe of the conformational properties of DNA because its emission intensity and FD are influenced by its local structural and solvation environments.[16] It can form a base pair with thymine with minimal disruption of the native DNA structure[17] and it can be selectively excited in the presence of tryptophan or tyrosine residues.[18] 2AP has been used to study the base-flipping actions of enzymes such as DNA methyltransferases.[16,19] It has also been used to study helicase activity,[20] the folding of ribozymes,[21] and DNA polymerase reactions.[22]

The lifetime distribution analysis has been carried out on FD data for 2AP in water–dioxane mixtures, 2AP in a dinucleotide, and 2AP in DNA duplexes. In these cases 2AP is expected to access a range of molecular conformations and solvation environments and so this selection will provide a critical test of the new protocol being proposed here. It will be shown that the new model distributions give sufficient flexibility to fit the apparent lifetime distribution while limiting the number of peaks (and hence distinct conformations/environments) to within physically justifiable limits. The results presented herein are chosen primarily to test the performance of the new methodology. Future publications will focus on its application to new problems of primary (bio)chemical interest.

An important physical artefact in FD data arises from the limited time resolution of the instrumentation. The measured FD is, in fact, a convolution of the true FD with a measured instrument response function (IRF). In current analysis software, the user inputs a fitting function for the true FD and this is convoluted and fitted against the measured FD.[23] It would be highly desirable instead to fit the true FD directly but this involves deconvolution of the experimental data. McKinnon *et al.* surveyed a number of commonly employed deconvolution methods.[24] Unfortunately, many of the more obvious approaches—such as by using Fourier transforms—are severely limited in their range of application due to well-known numerical problems such as truncation errors.[25] In this work, a new technique is proposed that yields reliable estimates of the true FD with no reliance on Fourier transforms and no restriction on the form of the FD. The method is based on a simulated annealing (SA) optimization of the true FD to yield, after convolution with the IRF, a best fit to the measured FD. Ideally the IRF should be measured under exactly the same experimental conditions as the corresponding FDs. In practice, the IRF is usually determined by recording the temporal profile of the excitation pulse by scattering the excitation light from a suspension of non-fluorescent particles, such as colloidal silica. The consequent difference in measurement wavelength between the IRF and the FD is not a problem if the time response of the detector has negligible dependence on wavelength, as is the case for the microchannel-plate multiplier tube used in the present work. However, the temporal responses of some detectors, notably avalanche diodes that are commonly used in time-resolved fluorescence microscopy and lifetime imaging, depend strongly on wavelength and the IRF is only valid if measured at a wavelength close to that of the FD. This can be achieved by using a reference fluorophore with a very short lifetime, as described in ref. 26. Alternatively, the problem may be circumvented by generating a synthetic IRF, as proposed by Večeř *et al.*[27,28] The present deconvolution method can be turned around to determine the IRF from the measured decay of any fluorophore of known lifetime; an example will be given in this work. The method may also be applied in cases such as fluorescence lifetime imaging microscopy, where the measurement of the IRF may be problematic.

This article is organised as follows. The deconvolution methodology and subsequent analysis of FD data are described in section II. Section III A reports the results from tests of the deconvolution methodology, showing that the technique is robust and gives identical information to conventional approaches. An example of determining an IRF by the simulated-annealing method is reported in section III B. Sections III C–III E report analyses of FDs of 2AP in water–dioxane mixtures, in a dinucleotide, and in DNA duplexes, respectively. The conclusions and an outlook on future applications of the new methodology appear in section IV.

2. Methodology and analysis

A. Deconvolution by simulated annealing

The FD from the fluorophore is measured as a discrete time series I_t. Typically, measurements are taken by photon counting until one of the time channels has accumulated 10 000 counts. The property of primary interest is the true FD which is denoted by F_t. I_t and F_t are related by a convolution with the IRF, denoted by $R_{t-t'}$:

$$I_t = \sum_{t' \le t} F_{t'} R_{t-t'} \equiv (F * R)_t \qquad (1)$$

The IRF is conveniently considered as obeying the normalization condition $\sum_{t \ge t'} R_{t-t'} = 1$. The IRF is measured experimentally as a function R_t while in fact it is a 'memory function' which should depend only on $t-t'$. Because the IRF and I_t are measured in separate experiments, there is inevitably a small difference in time origins. Therefore, the IRF has to be shifted relative to the measured I_t before deconvolution. Given a trial F_t, the shift is determined by trial and error to give the best agreement between I_t and $(F * R)_t$ over the first few time channels where the IRF has the greatest influence regardless of the precise choice for F_t. In practice, this shift is around 0.01 ns; in the experimental results analysed here, this represents only one or two time channels. All current fluorescence-analysis software accommodates such an offset.

The aim of the simulated annealing approach is to optimise F_t such that it provides, after convolution, the 'best fit' to I_t. The best fit was identified using a weighted, least-squares measure defined by

$$E = \frac{1}{N_t} \sum_t \frac{(I_t^{\mathrm{est}} - I_t)^2}{\sqrt{I_t}} \qquad (2)$$

where N_t is the number of points in the time series and I^{est}_t is the best estimate for F_t, convoluted with the IRF. The weighting factor is derived from the estimated statistical error in I_t assuming Poisson

statistics; this error is $\sim\sqrt{I_t}$ and so the weighting is $1/\sqrt{I_t}$. Note that E is not equal to a conventional weighted sum of the squares of residuals (WSSR), in which the weighting factor is the reciprocal of the variance (equal to I_t in Poisson statistics). Some tests were conducted using the WSSR as a least-squares parameter, but it was found that although the tail of the true FD could be determined precisely, the short-time portion of F_t was effectively unconstrained and led to extremely noisy results. F_t is optimised according to the following procedure. F_t is initialised by fitting a single exponential to the tail of the measured FD I_t. Then, a time point is selected in sequence and the corresponding value of F_t is multiplied by a random factor chosen uniformly from the range $\{e^{-\varepsilon}, e^{\varepsilon}\}$, where ε is a control parameter that is adjusted as the calculation proceeds. This is equivalent to a random displacement of $\ln F_t$ in the interval $\{-\varepsilon, \varepsilon\}$; it is the best option given that F_t spans several orders of magnitude. A change in F_t results in a change in the least-squares measure, denoted by ΔE. The random multiplication is accepted with a probability

$$p = \min (1, e^{-\Delta E/T}) \qquad (3)$$

where T is another control parameter. If $\Delta E < 0$ then $p = 1$ and the multiplication is accepted. If $\Delta E > 0$ then a random number r is chosen uniformly from the interval $\{0,1\}$: if $r \leq p$ then the multiplication is accepted; if $r > p$ then the multiplication is rejected and the old value of F_t is restored. This is basically a Metropolis Monte Carlo algorithm where E plays the role of energy and T is a temperature.[29] The SA procedure is effected through a gradual decrease in the temperature T and a reduction in the associated maximum-displacement parameter ε, which (hopefully) directs F_t towards the global minimum in E.[25] There is considerable flexibility in the choice of cooling schedule and so the following parameter choices may not be optimal. To begin with, $\varepsilon \simeq 0.005$ and T is set at a value of order $E_0/100N_t$ where E_0 is the value of the least-squares parameter at the start of the calculation; this was found to result in roughly 50% of attempted trial moves to be accepted. One sweep is defined as the multiplication (whether accepted or rejected) of each of the N_t time points. After 50 sweeps, both the temperature T and displacement parameter ε are reduced by a factor of 0.99. The cooling schedule is followed until I^{est}_t and I_t coincide within some pre-defined tolerance, usually a fraction of the natural scatter in the measured I_t. Note that other numerical optimisation strategies—such as the simplex method or the Levenberg–Marquardt (LM) algorithm[25]—would not be efficient for this particular application as there are too many degrees of freedom. In the case of the LM algorithm, for example, the required matrix diagonalisations would be prohibitively expensive.

B. Decay-constant distribution analysis

A common approach to fitting a complicated FD is to represent the true FD with a lifetime distribution

$$\frac{F_t}{F_0} = \int_0^\infty p(\tau) e^{-t/\tau} \mathrm{d}\tau \tag{4}$$

where τ is the lifetime and $p(\tau)$ is the corresponding probability density. In the conventional, multi-exponential fit $p(\tau)$ is effectively a weighted sum of δfunctions, $p(\tau) = \sum_{i=1}^{n} w_i \delta(\tau - \tau_i)$,giving

$$\frac{F_t}{F_0} = \sum_{i=1}^{n} w_i e^{-t/\tau_i} \tag{5}$$

where w_i is the contribution of lifetime i and $\sum_{i=1}^{n} w_i = 1$. The key step in the new model is to represent $p(\tau)$ as a continuous function with a sum of unimodal distributions of finite width, where each distribution represents a photophysically distinct population. There are many choices for these distributions and in addition there is the option of representing either a distribution of lifetime τ or a distribution of decay constant $k = 1/\tau$. Albery *et al.* have argued that one should consider a distribution of k since this is related to deviations in the activation free-energy.[8] It was shown that current transients in semiconductors, transient optical absorbance in colloidal semiconductors, redox kinetics in solid oxides, and the FD of a membrane -bound dye can all be described with a single Gaussian peak in $p(k)$ with dispersion. A fluorescence decay-constant distribution has been used subsequently by some authors.[30] In any case, if the ultimate conclusions regarding the number, positions, and breadths of peaks in the lifetime (or decay constant) distribution are to be taken as being physically reliable, then they should at least be independent of whether one has fitted distributions in k or τ. Certainly, in the current work, it is more convenient to work with a distribution $p(k)$:

$$p(k) = \sum_{i=1}^{n} w_i p_i(k) \tag{6}$$

I. Γ distribution: As for the form of the unimodal distributions, $p_i(k)$, Gaussian, Lorentzian, and log-normal functions immediately come to mind. The Gaussian distribution has the disadvantage that it is not naturally bounded to the region $0 \leq k \leq \infty$; it is not possible for a FD to possess a $k = 0$ ($\tau = \infty$) component. The same problem afflicts the Lorentzian distribution used by some groups [11] but in fact this choice is even more pathological because the distribution does not possess a properly defined statistical mean or variance. The log-normal distribution gets around these problems but it is inconvenient for analytical work. A flexible and simple form for $p_i(k)$ is the Γ distribution

$$p_i(k) = \frac{1}{\Gamma(\alpha_i + 1)\kappa_i} \left(\frac{k}{\kappa_i} \right)^{\alpha_i} e^{-k/\kappa_i} \tag{7}$$

where α_i and κ_i are shape and scale parameters, respectively, and $\Gamma(z)$ is the Gamma function.[15] The mode, the mean, and the variance of the decay constant, respectively, are given by

$$k_i^* = \alpha_i \kappa_i \tag{8}$$

$$\langle k \rangle_i = (\alpha_i + 1)\kappa_i \tag{9}$$

$$\langle k^2 \rangle_i - \langle k \rangle^2_i = (\alpha_i + 1)\kappa^2_i \tag{10}$$

The corresponding lifetime distribution $\tilde{p}_i(\tau)$ is related to $p_i(k)$ by

$$\tilde{p}_i(\tau) = \frac{p_i(\tau^{-1})}{\tau^2} \tag{11}$$

[Here a tilde over a probability density distribution function $p(x)$ denotes that it is derived from a modeled distribution $p(x^{-1})$.] The mode, the mean, and the variance of the lifetime, respectively, are given by

$$\tau_i^* = \frac{1}{(\alpha_i + 2)\kappa_i} \tag{12}$$

$$\langle \tau \rangle_i = \left\langle \frac{1}{k} \right\rangle_i = \frac{1}{\alpha_i \kappa_i} \tag{13}$$

$$\langle \tau^2 \rangle_i - \langle \tau \rangle_i^2 = \left\langle \frac{1}{k^2} \right\rangle_i - \left\langle \frac{1}{k} \right\rangle_i^2 = \frac{1}{\alpha_i^2(\alpha_i - 1)\kappa_i^2} \tag{14}$$

Representing $p_i(k)$ by eqn (7) leads to a particularly simple expression for the corresponding FD :

$$\int_0^\infty p_i(k) e^{-kt} \mathrm{d}k = \frac{1}{(1+\kappa_i t)^{\alpha_i + 1}}. \tag{15}$$

In the limit $\alpha_i \to \infty$ with $(\alpha_i + 1)\kappa_i$ constant, $1/(1 + \kappa_i t)^{\alpha_i + 1} \approx \exp[-(\alpha_i + 1)\kappa_i t] = \exp(-\langle k \rangle_i t)$. In other words, the Γ distribution accommodates the limit of a discrete lifetime, as used in eqn (5).

II. The general case: In numerical work, if the fitted value of α_i becomes very large, then the Γ distribution is very sharp and it is more conveniently represented by a δ function (and hence its contribution to F_t will be exponential). In the most general case $p(k)$ can be represented by the superposition in eqn (6) using n Γ distributions and m δ functions:

$$p(k) = \sum_{i=1}^{n} \frac{w_i}{\Gamma(\alpha_i + 1)\kappa_i} \left(\frac{k}{\kappa_i}\right)^{\alpha_i} e^{-k/\kappa_i} + \sum_{i=n+1}^{n+m} w_i \delta(k - k_i) \quad (16)$$

The general fitting function used in this work is therefore

$$\frac{F_t}{F_0} = \int_0^\infty p(k) e^{-kt} \mathrm{d}k = \sum_{i=1}^{n} \frac{w_i}{(1 + \kappa_i t)^{\alpha_i + 1}} + \sum_{i=n+1}^{n+m} w_i e^{-k_i t} \quad (17)$$

where of course $\sum^{n+m}_{i=1} w_i = 1$. A convenient label for the fit is $n\Gamma + m\delta$. Note that this approach is not restricted to simple exponential decays. For instance, it is perfectly possible to use stretched-exponential decays of the form $\exp[-(kt)^{\beta}]$, where β is a general exponent, either alone or in combination with an assumed distribution function $p(k)$. Another way of representing the true FD is to use an expansion in Laguerre polynomials and to fit to experimental data by varying the expansion coefficients.[31] Maarek *et al.* used such expansions to analyse the highly complex FDs of elastin,collagen, and cholesterol from time-resolved fluorescence spectra.[32] A benefit of the current approach is that the resulting expression for F_t (17) is extremely simple but is not constrained to be exponential.

C. Experimental procedure

FDs were measured by time-correlated single photon counting (TCSPC) on an Edinburgh Instruments TCC900 spectrometer using a procedure that has been described previously.[16,19] Decay data were recorded on a 50 ns timescale resolved into 4096 channels, to a total of 10 000 counts in the peak channel. The IRF of the system had a full width at half maximum (FWHM) of 70 ps. All solutions were prepared with analytical-grade solventsand all measurements were taken at a temperature of 298 K.

2-aminopurine and 2-aminopurine riboside were purchased from Sigma-Aldrich Ltd and Carbosynth Ltd, respectively, and used as received. 2-aminopurine-guanine dinucleotide was purchased from New England Biolabs Inc and used as received.

3. Results and discussion

A. Test of deconvolution by simulated annealing

The SA approach to deconvolution was tested by applying it to some artificially generated FDs. Figure 1 shows a model FD generated as a sum of four exponentials [as in eqn (5)] with lifetimes and weights typical for 2AP in a dinucleotide or a duplex. The model FDs (F^{model}_t) were convoluted with real IRFs and the results were used as 'experimental' I_ts for the simulated annealing method outlined in section II A. (The final results for I^{est}_t are essentially identical to I_t and show no apparent discrepancies when plotted on a linear-log scale, as will be done throughout.) Figure 1 shows the function F_t determined by SA, along with the initial input model FD. Clearly, there is some noise in F_t which arises from both the numerical accuracy of the simulated annealing procedure and the inherent noise in the IRF. This has to be quantified in order to weight properly the subsequent fitting analysis.

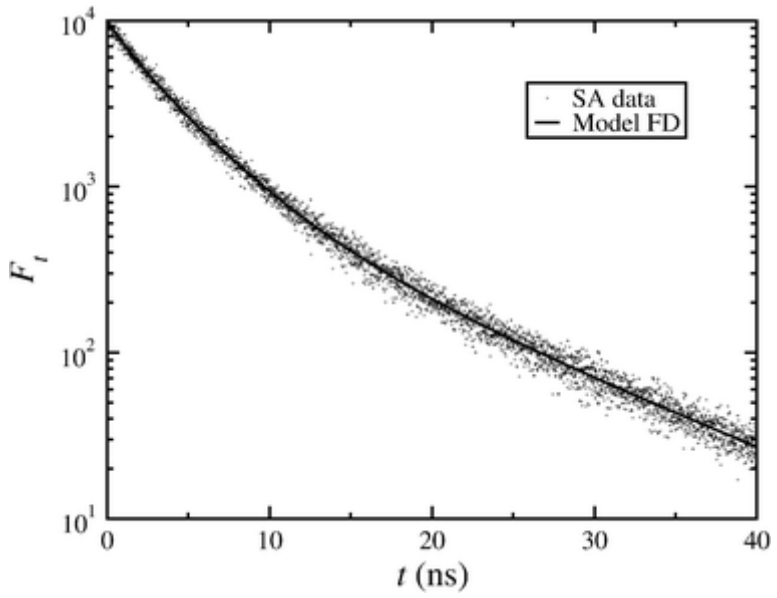

Figure 1. A comparison of a model FD (line) with the result of deconvolution by SA (points). The model FD is given eqn (5) with the following parameters: F_0 = 10 000; w_1 = 0.1; τ_1 = 11.0 ns; w_2 = 0.6; τ_2 = 3.2 ns;w_3 = 0.2; τ_3 = 5.0 ns; w_4 = 0.1; τ_4 = 0.9 ns.

Assuming Poisson statistics, the variance of the signal in each channel is equal to the mean (of which F_t is an estimate):

$$\langle \delta F^2_t \rangle = F_t \qquad (18)$$

The simulated annealing procedure introduces an additional error which may or may not be greater than the Poisson error. Figure 2 shows an example scatter plot (with logarithmic scales) of the squared deviations

$$\delta F^2_t = (F_t - F^{\text{model}}_t)^2 \qquad (19)$$

against F_t, the specific example is the same as that shown in Figure 1. Also shown is the Poisson variance (18). At low counts, the Poisson variance is larger than the SA squared deviations, while at high counts the SA deviations are dominant. The SA squared deviations were analysed from six modelFDs ; the results plotted on log–log scales suggest a straight line with a slope roughly equal to 2. The squared deviations for all six models were fitted simultaneously to yield the variance

$$\langle \delta F^2_t \rangle = 0.011 F^2_t \qquad (20)$$

In all of the subsequent fitting, the weighting factor for each point is $1/\sqrt{\langle \delta F_t^2 \rangle}$; the total variance as a function of F_t is given by a sum of the two contributions given in eqn (18) and (20).

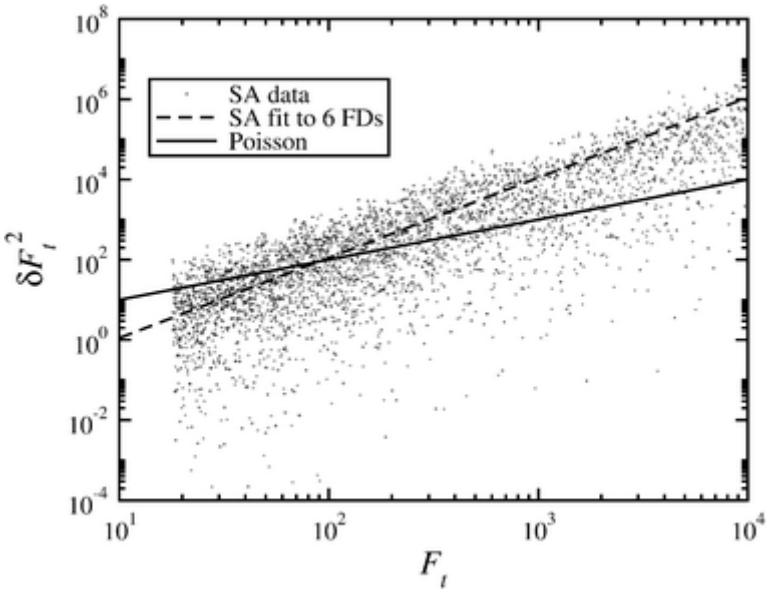

Figure 2. The Poisson variance and SA squared deviations plotted against $F_t$for the same model FD shown in Figure 1. The Poisson variance is given byeqn (18) while the SA average squared deviation (variance) from six model FDs was found to be eqn (20).

Other tests of the procedure were performed by comparing exponential fits of F_t obtained by SA to those produced by commercial FD analysis software. As an example, single-exponential fits of the form $F_t = F_0 \exp(-t/\tau)$ were performed to the FD of 10–20 μM 2AP(aq) at an emission wavelength of

380 nm. The commercial iterative convolution software FAST [33] [which fits $(F*R)_t$ to I_t] gave the lifetime $\tau = 11.774 \pm 0.010$ ns, while fitting a single exponential directly to the deconvoluted F_t obtained by SA yielded $\tau = 11.85 \pm 0.10$ ns (a difference of less than 1%).

B. Obtaining an IRF by simulated annealing

The SA algorithm can be employed to determine an IRF (R_t) from a measured FD (I_t) provided a true FD (F_t) is already known. The procedure outlined in Section II A is followed but now with an optimization of R_t rather than F_t. As an example, the true FD of 2 μM rhodamine-6G (R6G) in aqueous solution at $T = 295$ K is known to be a simple, single exponential with a lifetime of 4.08 ns at an emission wavelength of 558 nm.[34,35] The FD of 1 μM R6G (aq) was measured using TCSPC with an excitation wavelength of 455 nm and an emission wavelength of 555 nm. An IRF was measured for comparison with the results from SA. A fit to the tail of the measured I_t gave a lifetime of $\tau = 4.08$ ns in perfect correspondence with ref. 34 and 35; the true FD was then taken to be $F_t = F_0 \exp(-t/\tau)$. In the SA procedure, the initial guess for the IRF was a narrow Gaussian function plus a broad and shifted Gaussian to mimic a long-time tail.

Figure 3(a) shows the measured IRF along with the converged result from SA (with each result normalised to unit area); the agreement between $R_t$from the two approaches is excellent. The convolution $(F*R)_t$ shows excellent agreement with the FD measured directly in experiment (I_t); the results are shown in Figure 3(b) and (c) shows the deviations $(F*R)_t - I_t$. The maximum deviation is about 200 counts out of 10^4, representing a maximum scatter of only a few per cent which arises predominantly from noise in the measured FD.

(turn to next page →)

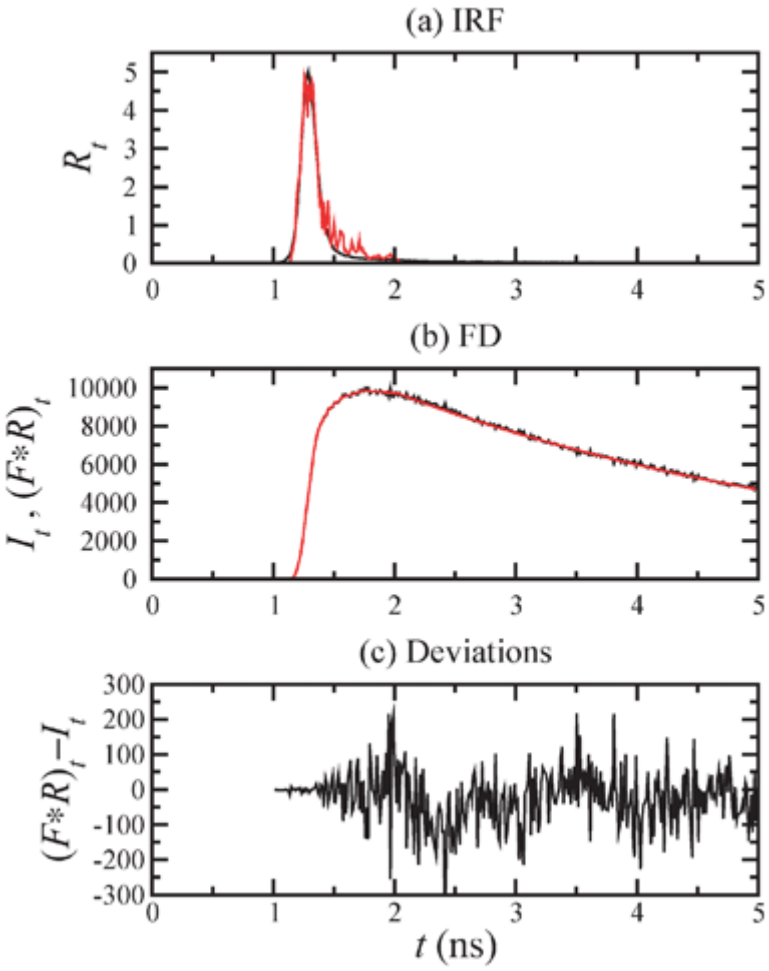

Figure 3. (a) IRFs obtained by direct measurement (black line) and by SA(red line). The two functions are each normalised to unit area. (b) Experimental FD of R6G (aq) (black line) along with the convolution of the true FD $F_t = F_0 \exp(-t/\tau)$ ($\tau = 4.08$ ns) with the IRF obtained from SA (red line). (c) The deviations $^{(F*R)_t} - I_t$.

C. Analysis of 2AP in water–dioxane

Bharill *et al.* analysed the FDs of 2AP in water–dioxane mixtures using single Lorentzian functions for the lifetime distributions

$$p(\tau) = \frac{(\gamma/2\pi)}{(\tau - \tau^*)^2 + (\gamma/2)^2} \qquad (21)$$

where γ is the FWHM and τ^* is the mode.[11] Notwithstanding the pathologies of the Lorentzian distribution, the lifetime distribution appears to vary systematically with the solvent composition. Specifically, Bharill *et al.* observed that γ shows a maximum around 40% v/v water in dioxane and attributed this to the "microenvironmental heterogeneity of the 2AP sample" arising from the solvent

mixture. This simple interpretation of the results does not take into account the fact that τ^* itself is a strong function of solvent composition; it increases by an order of magnitude between pure dioxane and pure water. The proper measure of heterogeneity should be the relative spread of lifetimes. As mentioned in Section II B, the results should not depend on whether one considers $p(\tau)$ or $\tilde{p}(k)$ which is derived from it. For the Lorentzian distribution given in eqn (21), the corresponding distribution of the decay constant is

$$\tilde{p}(k) = \frac{p(k^{-1})}{k^2} = \frac{(\gamma/2\pi)}{(1-k\tau^*)^2 + (\gamma k/2)^2} \qquad (22)$$

which has mode $\tau^*/[(\tau^*)^2 + (\gamma/2)^2]$ and FWHM $\gamma/[(\tau^*)^2 + (\gamma/2)^2]$. Hence, the ratio of the FWHM to the mode is the same for both $p(\tau)$ and $\tilde{p}(k)$ and is given by γ/τ^*—a correct measure for the spread. Table 1 shows the Lorentzian fitting parameters reported in ref. 11 along with the relative spread of the distribution. The variation of γ/τ^* with solvent composition is much less pronounced and regular than that of γ itself and shows a precipitous drop between 40% and 50% v/v water in dioxane. Note that the standard deviation of $p(\tau)$—an alternative measure of the absolute spread—is undefined for the Lorentzian distribution.

% water	**τ^*/ns**	**γ/ns**	**γ/τ^***
0	1.48 ± 0.00383	0.30 ± 0.0218	0.203 ± 0.015
2	2.55 ± 0.00628	0.59 ± 0.0031	0.2314 ± 0.0013
10	5.41 ± 0.0137	1.50 ± 0.0616	0.277 ± 0.011
20	6.58 ± 0.0174	1.79 ± 0.0774	0.272 ± 0.012
40	7.68 ± 0.0207	2.16 ± 0.0860	0.281 ± 0.011
50	10.65 ± 0.0452	1.21 ± 0.0540	0.1136 ± 0.0051
75	11.38 ± 0.0345	0.83 ± 0.0481	0.0729 ± 0.0042
100	11.89 ± 0.0548	0.70 ± 0.0213	0.0589 ± 0.0018

Table 1. Single Lorentzian fitting parameters for 2AP in water–dioxane mixtures as reported in ref. 11: τ^* is the mode of the Lorentzian lifetime distribution; γ is the full width at half maximum; the values and ± errors are reproduced precisely as they appear in ref. 11. The ratio γ/τ^* measures the relative spread of the distribution since the moments of the Lorentzian distribution are undefined.

New FDs were measured for 2AP in water–dioxane solvents with selected compositions (0%, 10%, 20%, and 100% v/v water in dioxane). In addition, results were also obtained for 2AP with 2-deoxyribose attached (2APr). In all cases the excitation wavelength was 305 nm and the emission

wavelength was 380 nm. The true FDs resulting from SA were fitted in the first instance using single Γ distributions for $p(k)$, *i.e.*, 1Γ fits. The measured and true FDs for 2AP are shown in Figure 4.

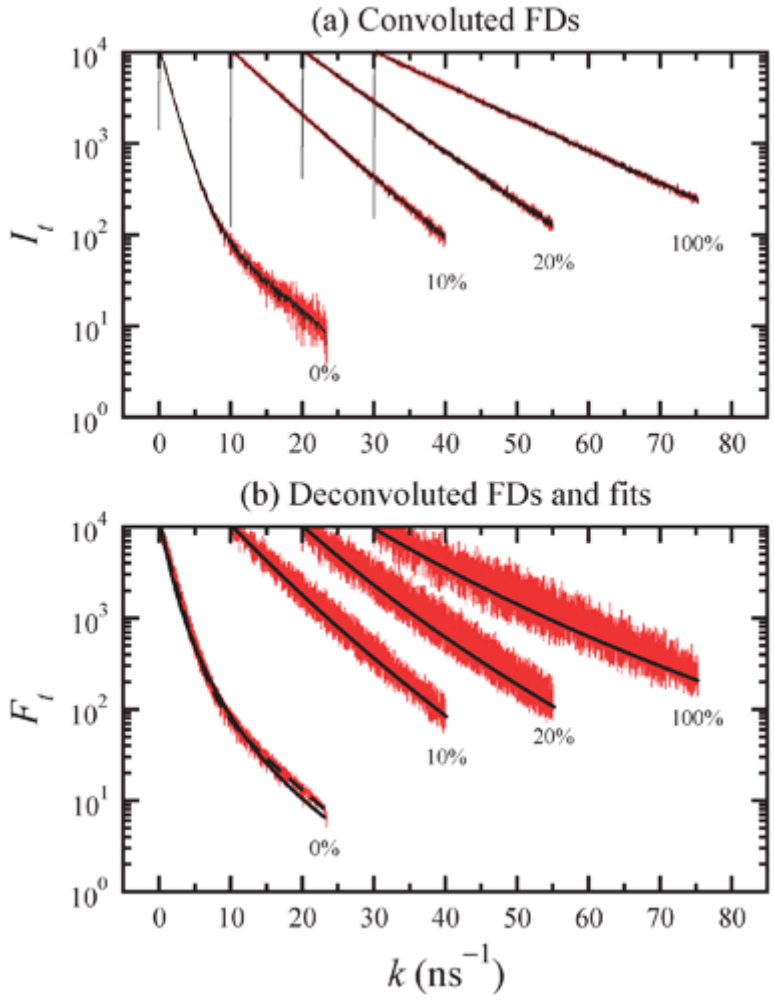

Figure 4. FDs for 2AP in water–dioxane mixtures with compositions of (from left to right) 0%, 10%, 20%, and 100% water v/v. (a) I_t as measured directly in experiments (red lines) and the convoluted best-fit $(F * R)_t$ (black lines) where F_t is the apparent true FD decay from SA and R_t is the IRF. (b) Apparent true FD decays (F_t) from SA (red lines) and the associated 1Γ fits (black lines). A 1Γ + 1δ fit for pure dioxane is shown as a black dashed line.

Figure 5 shows the resulting $p(k)$ for 2AP. For comparison, Figure 5 also shows $\tilde{p}(k)$s obtained from the Lorentzian $p(\tau)$s reported in ref. 11 for 2AP in the same solvents. In qualitative terms, the two sets of results are comparable, showing the same trend in peak position with changing solvent composition. Table 2 shows the parameters and associated moments from the 1Γ fits to both 2AP and 2APr. The average lifetimes $\langle\tau\rangle$ derived from fitted $p(k)$s are in reasonable agreement with the

modes reported by Bharill *et al.*,[11] varying by a factor of 10 between pure dioxane and pure water. Appropriate measures of the spreads of k and τ are $\sigma_k / \langle k \rangle$ and $\sigma_\tau / \langle \tau \rangle$, respectively, where σ_k and σ_τ are the corresponding standard deviations [square-roots of the variances given in eqn (10) and (14)]. Whether one considers distributions in k or τ, a consistent measure of spread is obtained. The results for 10%, 20%, and 100% v/v water in dioxane show only a weak variation. The spreads in pure dioxane appear to be anomalously high, which can be traced to a simple 1Γ fit being inadequate for this particular case.

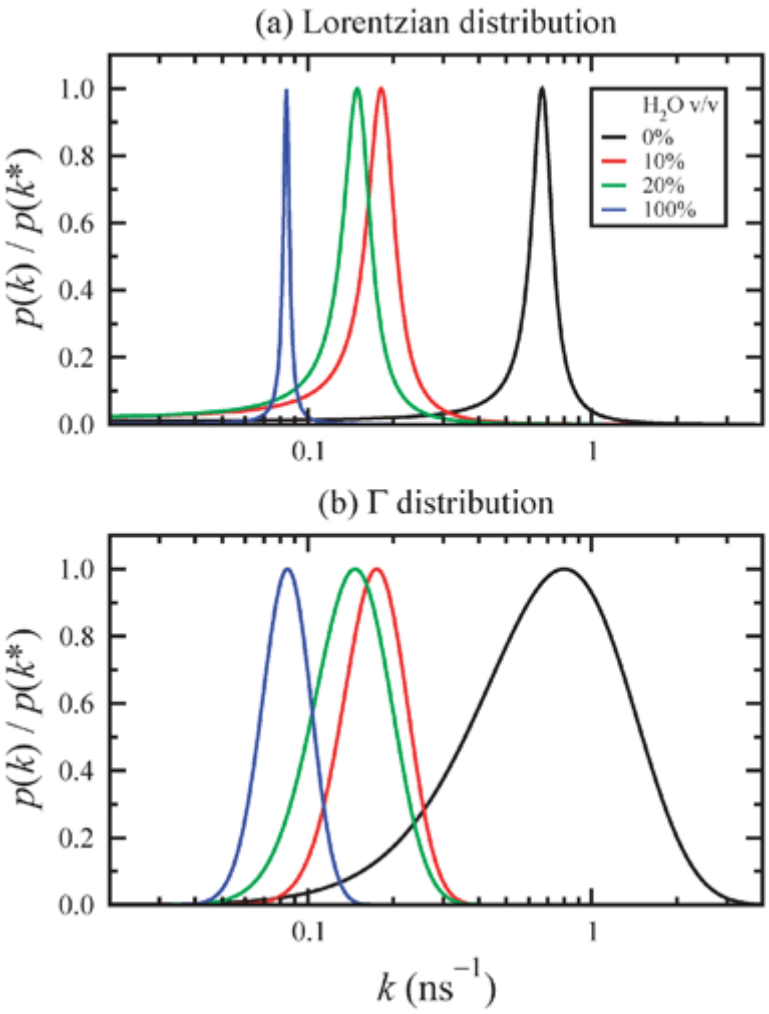

Figure 5. Decay-constant distributions for 2AP in water–dioxane. (a) Apparent decay-constant distributions determined using the fitted Lorentzian lifetime distributions reported in ref. 11. (b) Results of 1Γ fits to F_t extracted by SA from new experimental measurements. k^* is the mode of the distribution (position of the maximum).

% Water v/v	α	κ/ns^{-1}	$\langle k \rangle$ /ns^{-1}	$\sigma_k / \langle k \rangle$	$\langle \tau \rangle$ /ns	$\sigma_\tau / \langle \tau \rangle$	χ^2_r
2AP							
0	2.754 ± 0.046	0.2905 ± 0.0079	1.091 ± 0.032	0.516 ± 0.021	1.250 ± 0.040	0.755 ± 0.032	2.07
10	15.2 ± 1.6	0.0115 ± 0.0013	0.187 ± 0.028	0.248 ± 0.048	5.69 ± 0.87	0.265 ± 0.052	4.55
20	10.4 ± 1.5	0.0141 ± 0.0022	0.160 ± 0.033	0.296 ± 0.078	6.9 ± 1.4	0.327 ± 0.088	8.37
100	25.7 ± 2.0	0.00329 ± 0.00028	0.088 ± 0.010	0.193 ± 0.028	11.8 ± 1.4	0.201 ± 0.030	9.99
2APr							
0	19.8 ± 1.7	0.0185 ± 0.0017	0.385 ± 0.047	0.219 ± 0.034	2.73 ± 0.33	0.230 ± 0.037	2.70
10	36.8 ± 4.6	0.00458 ± 0.00059	0.173 ± 0.031	0.163 ± 0.037	5.9 ± 1.1	0.167 ± 0.038	2.40
20	34.7 ± 5.2	0.00394 ± 0.00060	0.141 ± 0.030	0.167 ± 0.045	7.3 ± 1.6	0.172 ± 0.047	4.98
100	49.0 ± 6.2	0.00197 ± 0.00026	0.098 ± 0.018	0.141 ± 0.033	10.4 ± 1.9	0.144 ± 0.034	2.45

Table 2. 1Γ fitting parameters for 2AP and 2APr in water–dioxane mixtures. α is the shape parameter and κ is the scale parameter. The ratio $\sigma_x / \langle x \rangle$ measures the relative spread of the distribution, where $\sigma^2_x = \langle x^2 \rangle - \langle x \rangle^2$

A reduced chi-squared parameter, χ^2_r, is defined to measure the 'goodness of fit'. χ^2_r is given by

$$\chi^2_r = \frac{1}{v}\sum_t \left(\frac{\delta F_t^2}{\langle \delta F_t^2 \rangle} \right) \qquad (23)$$

where δF^2_t is the squared deviation between fit and experiment and v is the number of degrees of freedom (number of fitted points minus the number of fit parameters minus 1). The denominators are each given by the sum of eqn (18) and (20) and, as explained in Section III A, they are only estimates based on a small sample of model cases. The squared deviations amongst these model cases are scattered by orders of magnitude and so χ^2_r can only be used for comparing different fits and not as an absolute measure of fit quality. Figure 6 shows weighted residuals $(\delta F_t / \sqrt{\langle \delta F_t^2 \rangle})$ for various fits to the FDs of 2AP in pure dioxane along with the overall χ^2_r parameter. Figure 6(a) and (c) show that single functions are not adequate for fitting, while 2δ and 1Γ + 1δ fits give acceptable and comparable

results. The resulting improvements in the fits—particularly in the tails—are visible in Figure 4. (Including more functions in the fits leads to uncertainties in the fit parameters of more than 100%.)

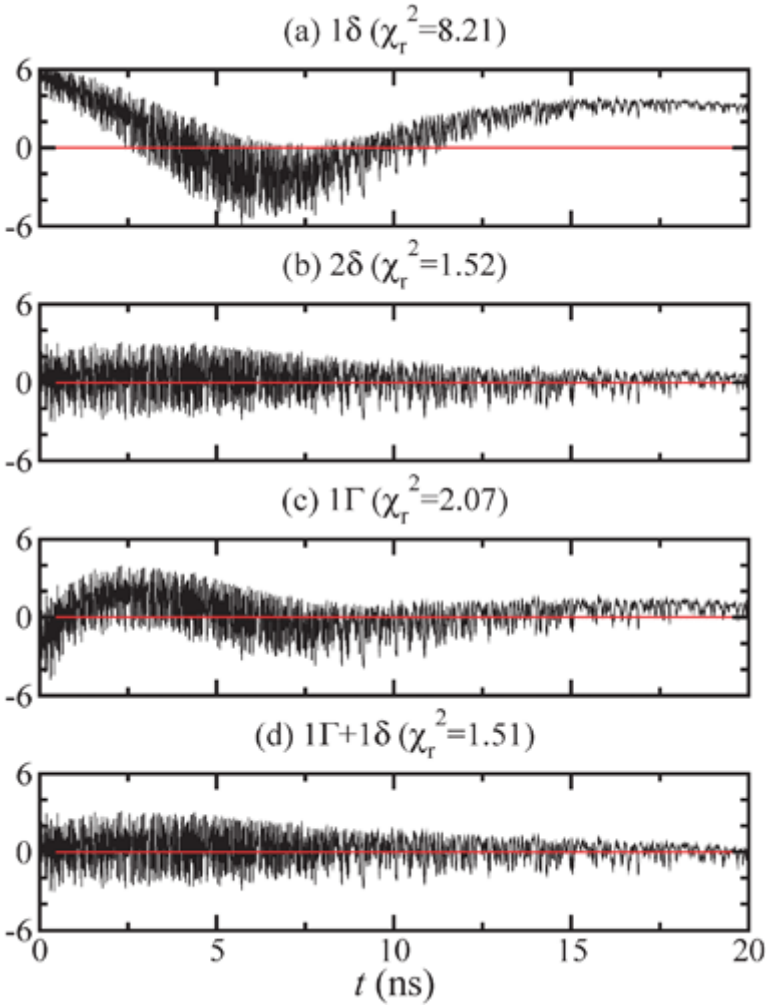

Figure 6. Weighted residuals $\delta F_t / \sqrt{\langle F_t^2 \rangle}$ from various fits to F_t for 2AP in pure dioxane: (a) 1δ; (b) 2δ; (c) 1Γ; (d) 1Γ + 1δ.

It is unclear why 2AP and 2APr should present more complex FDs in pure dioxane than in water–dioxane mixtures, although perhaps some solvent -mediated attraction between fluorophores leads to stacking or association, giving rise to an alternative pathway for quenching. Dioxane has a low dielectric constant of 2.2 and so in water–dioxane mixtures, it is possible that 2AP and 2APr are primarily solvated by water due to its high polarity and greater propensity for hydrogen bonding. Table 2 shows that in pure dioxane the mean decay constants from 1Γ fits are anomalously high. Solvent mediated stacking of 2AP could lead to an increase in the decay constant, similar to what

happens when 2AP stacks with the natural bases, particularly guanine;[36] this will be considered explicitly in the next section. 2AP shows a higher enhancement in the mean decay constant than 2APr, perhaps reflecting differences between the solvophobic attraction related to the presence of the 2-deoxyribose.

The results in this section show that 1Γ fits to the FDs of 2AP in water–dioxane mixtures provide average lifetimes that are comparable to those obtained with Lorentzian distributions.[11] In particular, the strong dependence on solvent composition can be determined reproducibly. A suitable measure of the relative spread of lifetimes can be defined which gives similar results irrespective of whether one considers the lifetime or the decay constant. In general, there does not appear to be a very strong dependence of this relative spread on solvent composition, apart from the case of pure dioxane. This can be traced back to the fact that a 1Γ fit is inadequate in this case; a 1Γ + 1δ fit does much better, although it is comparable to a 2δ(two-exponential) fit. No difficulties in fitting results for 2AP in pure dioxane were reported in ref. 11.

D. Analysis of 2AP in a dinucleotide

Ref. 11 and Table 2 show that 2AP in aqueous solution at room temperature has a mean fluorescence lifetime near the emission maximum of 11–12 ns. 2AP can be incorporated into DNA primarily as an analogue of adenine. When 2AP is base stacked in DNA, its fluorescence is highly quenched by charge transfer with the natural bases, particularly guanine.[37,38] In DNA duplexes, 2AP shows a complex FD that can be described by the sum of four exponential components with typical lifetimes of <0.1 ns, ~0.5 ns, ~2 ns, and ~10 ns.[16,17,36,39,40] It is generally accepted that the very fast component ($k > 10$ ns^{-1}) corresponds to a highly stacked conformation in which the excited 2AP is rapidly quenched by inter-base charge transfer, and that the very slow component ($k \sim 0.1$ ns^{-1}) is due to 2AP that is destacked from its neighbouring bases and exposed to solvent. The intermediate lifetimes are loosely attributed to partially stacked structures between these two extremes. This section and the next focus on the extent to which these fast, slow, and intermediate components can be described by distributions of decay constants. This section is devoted to the extremely simple case of a dinucleotide.

Fluorescence measurements have been performed on 2AP in a dinucleotide consisting of two linked phosphates, two ribosugars, one guanineresidue, and one 2AP residue. This simple system should admit at least two distinguishable conformations, with the 2AP and guanine either stacked or not. There is, however, a range of conformations which may exhibit different degrees of quenching. For instance, 2AP and guanine need not be stacked face-to-face; there may be a range of intermediate conformations involving weak edge-to-face or even edge-to-edge interactions.

Measurements were taken with an excitation wavelength of 305 nm and an emission wavelength of 380 nm. The true FD resulting from SA is sufficiently complex that conventional multi-exponential fits require many distinct lifetimes. The best multi-exponential fit (lowest χ^2_r and fit-parameter uncertainties <100%) required four distinct lifetimes (4δ fit, 8 fitting parameters). The fit parameters are given in Table 3.

i	w_i	k_i/ns^{-1}	τ_i/ns
Dinucleotide (χ^2_r = 6.88)			
1	0.41 ± 0.38	14.2 ± 15.2	0.070 ± 0.075
2	0.138 ± 0.086	1.5 ± 1.4	0.69 ± 0.65
3	0.40 ± 0.11	0.561 ± 0.053	1.78 ± 0.17
4	0.0522 ± 0.0020	0.0920 ± 0.0018	10.86 ± 0.21
Duplex (χ^2_r = 3.72)			
1	0.64 ± 0.32	46 ± 22	0.022 ± 0.011
2	0.210 ± 0.023	1.98 ± 0.32	0.505 ± 0.083
3	0.108 ± 0.011	0.429 ± 0.047	2.33 ± 0.26
4	0.0454 ± 0.0047	0.1290 ± 0.0055	7.75 ± 0.33
Duplex with enzyme (χ^2_r = 11.7)			
1	0.49 ± 0.19	7.1 ± 3.9	0.140 ± 0.077
2	0.337 ± 0.055	0.77 ± 0.20	1.30 ± 0.34
3	0.113 ± 0.044	0.242 ± 0.098	4.1 ± 1.7
4	0.061 ± 0.025	0.097 ± 0.012	10.4 ± 1.3

Table 3. 4δ fitting parameters for 2AP in a dinucleotide, and for 2AP in duplexes with and without enzyme.

By introducing a Γ function, the required number of δ functions could be reduced to two; the parameters from the resulting 1Γ + 2δ fit are given in Table 4. The optimum fitting function was determined in the following way. First, two Γ functions were fitted to the FD (2Γ fit, 6 fitting parameters). The quality of the fit was much poorer than that of the 4δ fit. One Γ function showed a very sharp peak at $k \simeq 19$ ns^{-1} and a very large value of αwhich is a clear indication that this could be represented with a δ function (see sections II B1 and II B2); the other Γ function was broad (small value of α) and was centred at a much smaller value of $k \simeq 0.6$ ns^{-1}. Next, a 1Γ + 1δ fit was attempted (5 fitting parameters), but this was still inferior to the 4δ fit. Finally, a 1Γ + 2δ fit (7 fitting

parameters) was found to give a value of χ^2_r which was almost identical to that from the 4δ fit but with one less fit parameter.

i	w_i	α_i	κ_i/ns^{-1}	$\langle k \rangle_i$/ns^{-1}	$\langle \tau \rangle_i$/ns
Dinucleotide (χ^2_r = 6.87)					
1	0.474 ± 0.033	4.6 ± 1.8	0.135 ± 0.053	0.76 ± 0.38	1.60 ± 0.88
2	0.49 ± 0.48	δ function		19 ± 16	0.053 ± 0.044
3	0.0361 ± 0.0038	δ function		0.0842 ± 0.0033	11.87 ± 0.47
Duplex (χ^2_r = 3.74)					
1	0.514 ± 0.060	1.00 ± 0.30	0.68 ± 0.23	1.36 ± 0.50	1.47 ± 0.66
2	0.40 ± 0.16	δ function		12.2 ± 6.7	0.082 ± 0.045
3	0.0826 ± 0.0063	δ function		0.157 ± 0.011	6.38 ± 0.47
Duplex with enzyme (χ^2_r = 11.7)					
1	0.49 ± 0.13	3.69 ± 0.44	0.137 ± 0.016	0.643 ± 0.096	1.98 ± 0.33
2	0.43 ± 0.17	δ function		4.5 ± 2.7	0.22 ± 0.14
3	0.086 ± 0.021	δ function		0.1041 ± 0.0035	9.60 ± 0.32

Table 4. 1Γ + 2δ fitting parameters for 2AP in a dinucleotide, and for 2AP in duplexes with and without enzyme. α is the shape parameter and κ is the scale parameter.

Some large uncertainties are given in Table 3 and 4, particularly in the parameters for the δ functions with high values of k (i = 1,2 in the 4δ fit and i= 2 in the 1Γ + 2δ fit). These arise from the fact that the FDs are analysed by weighted fits (as explained in section III A) and that the total variances in the FDs are estimated only very roughly [by eqn (18) and (20)]. The fitting uncertainties are therefore significantly overestimated.

Figure 7 shows the $p(k)$s arising from the 4δ and 1Γ + 2δ fits for the dinucleotide. The δ functions are shown as impulses with height w_i as reported in Table 3 and 4. (Some general comments on how to interpret such representations will be given in section III E1.) It is clear from both types of fit that there must be at least two pure-exponential decays, one fast and one slow; these have decay constants

$\sim$0.1 ns^{-1} and $\sim$10 ns^{-1} corresponding to de-stacked and stacked 2AP, respectively. The most significant feature is the way in which the different fits represent the contributions with 'intermediate' decay constants. The 4δ fit is constrained to indicate two distinct decay constants bracketed by the fast and slow ones. Although it is quite clear that a significant intermediate-k contribution is required, it is not physically obvious why two distinct decay constants should appear. What the 1Γ + 2δ fit indicates is that this intermediate range can be represented by a single broad feature which might represent a manifold of conformational states in which the 2AP is neither completely stacked with the guanine nor entirely de-stacked. From a purely numerical perspective, the 4δ and 1Γ + 2δ fits require eight and seven parameters, respectively, but the quality of fit is the same. Without any specific information on the likely conformational states of the dinucleotide, one has to conclude that the 1Γ + 2δ fit is at least as meaningful as the 4δ fit and is, in fact, more straightforward to understand on physical grounds since it indicates only one broad range of intermediate conformational states rather than two distinct conformations.

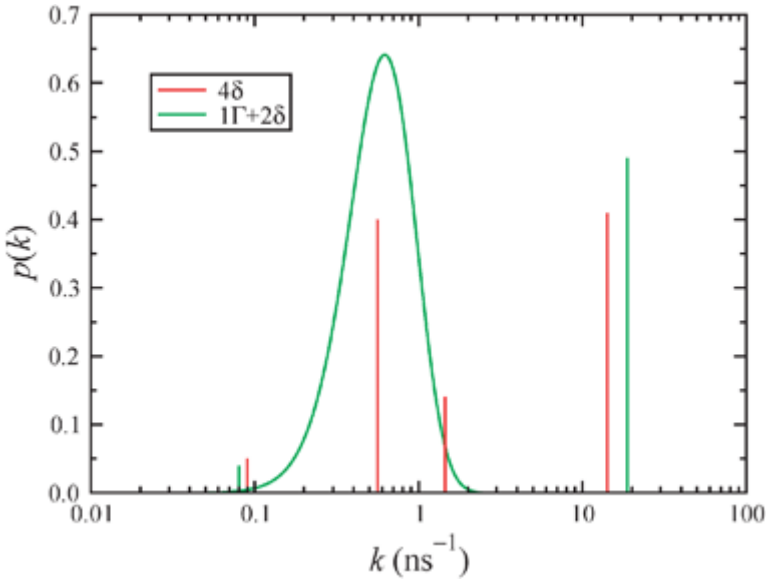

Figure 7. Decay-constant distributions for 2AP in a dinucleotide. The δ-functions are represented by impulses of height w_i as reported in Table 3 and 4.

E. Analysis of 2AP in a duplex

The results of the previous section show that the apparent $p(k)$ for 2AP in a dinucleotide consists of sharp peaks at low-k and high-k, and a broad distribution of intermediate decay constants. The next example shows that this feature is also observed for 2AP in a DNA duplex. This again casts some

doubt on the physical significance of fitting two intermediate lifetimes, as would be done in a 4δ fit. One strand of the duplex contains 2AP and its sequence is

5′-GGGGATCCTCTAGAGTCGACCTGCAGGGCPA-3′

where P denotes the 2AP in place of adenine. The other strand is complementary. The duplex can be bound to an enzyme which distorts the duplex structure and leads to de-stacking of 2AP and hence decreases the degree of quenching and the associated decay constant. These particular cases provide good tests of fitting procedures, because the FDs are apparently quite complex.

FD measurements were taken with an excitation wavelength of 305 nm and an emission wavelength of 380 nm. Using the conventional multi-exponential functions, four distinct lifetimes are required to achieve acceptable fits to the true FD ; 4δ fit parameters are shown in Table 3. The values of χ^2_r are 3.72 and 11.7 for the duplexes without and with enzyme, respectively. Table 4 reports the 1Γ + 2δ fitting parameters for the same FDs ; other combinations of Γ and δ functions were tested (as explained in section III D) but the 1Γ + 2δ combination gave the best fit. The values of χ^2_r are 3.74 and 11.7 for the duplexes without and with enzyme, respectively, so in terms of fit quality, this combination performs just as well as the 4δ fit but with one less adjustable parameter.

As anticipated, fast and slow components are seen corresponding to the stacked and de-stacked conformations of 2AP. The 4δ fit for the duplex by itself gives an extreme value for the decay constant of the fast (stacked-2AP) component, $k = 46$ ns^{-1} (albeit with a large uncertainty) which is far higher than the corresponding fast component in the dinucleotide ($k = 14$ ns^{-1}). The corresponding fast component in the 1Γ + 2δ fit shows a consistency between the duplex ($\langle k \rangle = 12$ ns^{-1}) and dinucleotide ($\langle k \rangle = 19$ ns^{-1}) cases. The decay-constant distributions are shown in Figure 8 and ostensibly tell the same story as for the dinucleotide. The slow and fast components are roughly equivalent in the 4δ and 1Γ + 2δ fits, but the major difference is again with the intermediate range of decay constants. As for the dinucleotide case, it is easier to justify this range as corresponding to one broad manifold of conformations between the stacked and de-stacked limits, than it is to argue for two distinct conformations.

(turn to next page →)

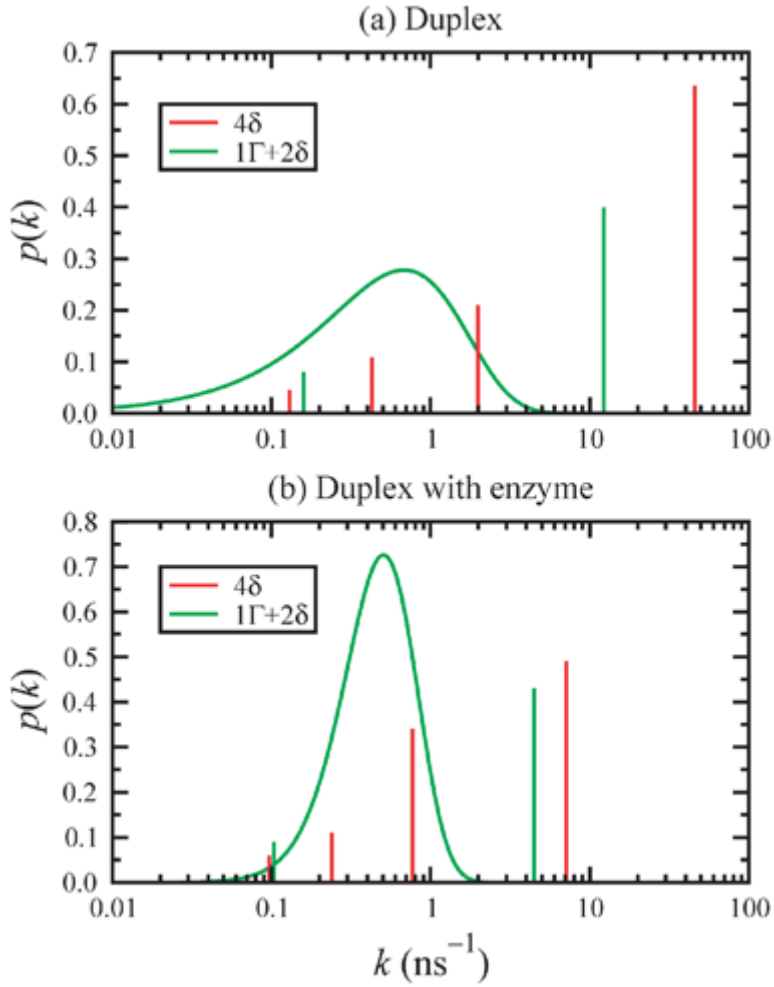

Figure 8. Decay-constant distributions for 2AP in a duplex. (a) Duplex without enzyme. (b) Duplex with enzyme. The δ functions are represented by impulses of height w_i as reported in Table 3 and 4.

Both fits show that the presence of enzyme reduces the decay constant of the fastest component, indicating a distortion of the duplex which reduces the quality of the stacking and hence the rate of quenching. Moreover, the decay-constant distributions clearly reveal the effects of enzyme binding on the conformations of the duplex, showing a transfer of the population from well-stacked ($k > 1$ ns^{-1}) to poorly stacked ($k < 1$ ns^{-1}) states.

I. Important comments on interpreting *n*Γ+*mδ* plots: Figure 7 and 8 represent $p(k)$ with the true contributions from the Γ functions but impulses of height w_i in place of the δ functions; the alternative is to show each δ function as just a vertical line with no indication of its area. The wide spreads of decay constants mean that the data are best presented with a logarithmic scale on the abscissa. These representations may, at first glance, lead to some misunderstandings and so it is important to highlight the shortcomings of the $n\Gamma + m\delta$ plots and to indicate how they should be read. There are three apparent problems in a plot such as Figure 8(a): the Γ function appears to show an anomalously long

low-k tail, reaching to unphysically low values of, say, $k < 0.05$ ns^{-1}; the impulses in place of the δ functions suggest that they are insignificant as compared to the broad peak of the Γ function; and the logarithmic scale on the abscissa makes it difficult to judge by eye the relative contributions from each of the functions. With specific reference to Figure 8(a), then, the following points should be noted. Looking at the Γ function contribution, the integrated probability from decay constants up to $k = 0.05$ ns^{-1} is by numerical integration equal to about 0.00132; hence, the apparent low-k tail is utterly insignificant. Secondly, the contribution from the δ function at $k = 0.157$ ns^{-1} is, from Table 4, $w_3 = 0.0826$ which is a factor of 7 greater than the contribution (0.0118) from the Γ function up to that value of k. Figure 9 shows the same data as in Figure 8 but with a linear scale on the abscissa and over the limited range $k \leq 4$ ns^{-1}. This plot illustrates that the apparent low-k tail in 8(a) is really just a graphical distortion of the data.

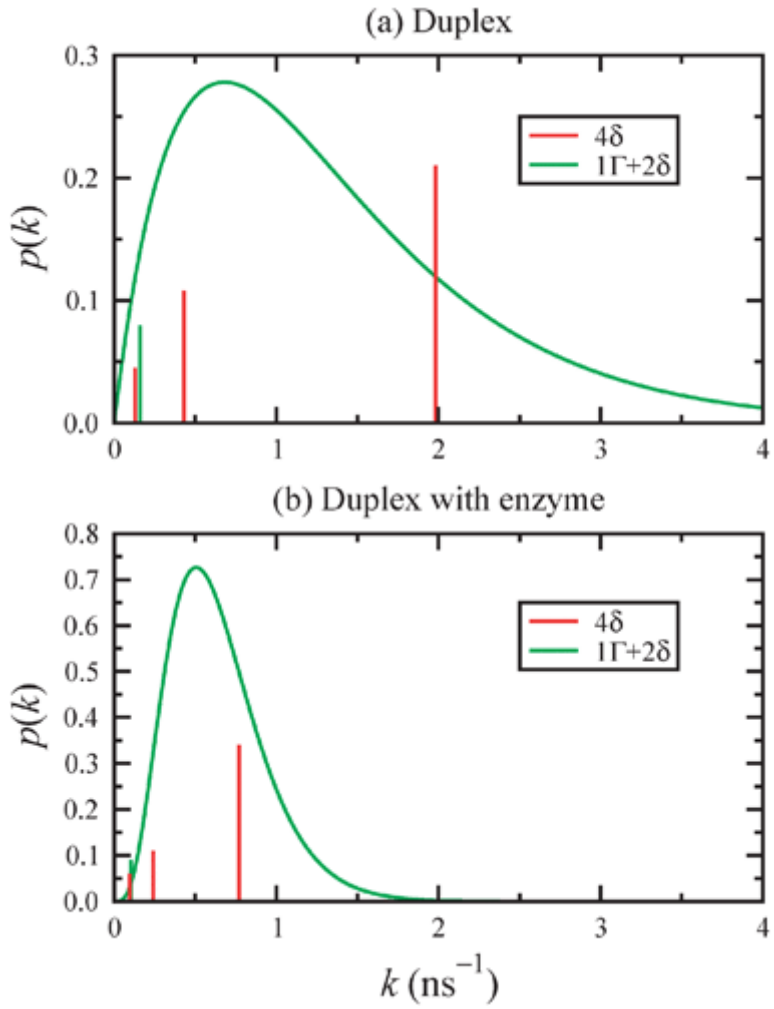

Figure 9. Decay-constant distributions for 2AP in a duplex shown on a linear scale in the range $k \leq 4$ ns^{-1}. (a) Duplex without enzyme. (b) Duplex with enzyme. The δ functions are represented by impulses of height w_i as reported in Table 3 and 4.

4. Conclusions

In this paper several important aspects of fluorescence decay analysis have been addressed. The first aspect concerns the way in which the effect of the instrument response function can be removed from an experimentally measured decay to yield the true decay. The true decay is desirable because it can be fitted directly with model fitting functions. It has been shown that a simulated annealing procedure can be used to extract the true decay with a precision sufficient to give results that are comparable with those from conventional approaches (namely, fitting a convoluted function to the experimental decay). The procedure can also be employed to extract an instrument response function, provided a true decay is known in advance. An example has been presented and the results are essentially identical to those from a direct measurement. The simulated annealing approach certainly works but it can be improved. One issue concerns the way in which the true decay is optimised, channel -by-channel ; this gives rise to a degree of scatter resembling statistical noise. This could be eliminated to some extent by describing the true decay as a set of smooth segments or splines, which are iterated; this will remove the short timescale noise but will also reduce the flexibility of the optimised function.

The second aspect concerns how true fluorescence decays can be fitted in a physically meaningful way. The conventional approach in complex situations—which are becoming increasingly common in biological applications—is to fit the decay with a sum of exponentials. One example presented here concerned the fluorescence of 2-aminopurine in water–dioxane mixtures and it was shown that the decay-constant distribution is fitted adequately with a single peak of finite width. With the exception of pure dioxane (which benefits from an additional exponential function) the breadths of the distributions are shown to vary monotonically with the solvent composition, in contrast to what was concluded in earlier work.[11] Two other situations were considered, involving 2-aminopurine in a dinucleotide and in DNA duplexes. The decays in these cases are sufficiently complex that, in the conventional approach, four distinct exponentials are required: two exponentials describe slow and fast decays, corresponding to 2-aminopurineeither de-stacked or stacked with its neighbour(s); the other two exponentials merely fill in contributions with intermediate decay constants, corresponding to conformations which are neither well stacked nor completely de-stacked. There is no physical reason why two distinct conformations or decay constants should be expected in this intermediate range. Fits of equal quality can be achieved with fewer fitting parameters by including two exponentials for the slow and fast decays and a non-exponential function derived from a single broad peak in the decay-constant distribution; it is easy to argue for a single manifold of intermediate conformations, not least by appealing to Occam's law of parsimony.

The main message here is that improvements can be made to multi-exponential fits that result in fewer fitting parameters and no reduction in fit quality. This involves fitting a broad, smooth distribution of decay constants in place of several distinct decay constants. This general strategy has been proposed

several times before but it is surprising that it has not yet been more widely adopted. For instance, Albery *et al.* used Gaussian decay-constant distributions to fit fluorescence decays and other transients, and concluded that, "the traditional application of multiexponential analysis to this type of curve may be mistaken and that [their] model provides a simpler and more realistic explanation."[8]

Finally, it should be noted that some of the issues discussed here are quite generic in physical chemistry; see ref. 8 for examples of other transient signals that can be analysed to yield decay-constant distributions. Förster resonance energy transfer (FRET) is a fluorescence technique that is widely used for the study of intermolecular interactions and macromolecular conformations in biomolecular systems, and one for which analysis in terms of a distribution of rate constants is acknowledged to be appropriate.[41] In FRET, electronic energy is transferred from an excited donor molecule to a ground-state acceptor molecule (over distances of <10 nm) at a rate that depends on the separation between the two. In molecular systems to which FRET is applied, there almost always exists a distribution of donor–acceptor distances[42,43] and hence a distribution of energy transfer rates which is manifested in the fluorescence decay of the donor as a distribution of decay constants. Also, in practical (non-ideal) FRET systems, there often exists a discrete population of donor molecules that does not experience energy transfer and retains the unquenched fluorescence lifetime. The present approach, in which the description of the decay in terms of a combination of discrete and distributed decay constants is implicit, should, therefore, be very appropriate for the analysis of FRET data.

References

[1] D. R. James and W. R. Ware, *Chem. Phys. Lett.*, 1985, **120**, 455–459.

[2] J. R. Alcala, E. Gratton and F. G. Prendergast, *Biophys. J.*, 1987, **51**, 587–596.

[3] A. Siemiarczuk and W. R. Ware, *J. Phys. Chem.*, 1987, **91**, 3677–3682.

[4] A. Siemiarczuk and W. R. Ware, *J. Phys. Chem.*, 1989, **93**, 7609–7618.

[5] Y. S. Liu and W. R. Ware, *J. Phys. Chem.*, 1993, **97**, 5980–5986.

[6] J. R. Lakowicz, H. Cherek, I. Gryczynski, N. Joshi and M. L. Johnson, *Biophys. Chem.*, 1987, **28**, 35–50.

[7] J. R. Alcala, E. Gratton and F. G. Prendergast, *Biophys. J.*, 1987, **51**, 597–604.

[8] W. J. Albery, P. N. Bartlett, C. P. Wilde and J. R. Darwent, *J. Am. Chem. Soc.*, 1985, **107**, 1854–1858.

[9] G. Verbeek, A. Vaes, M. Van der Auweraer, F. C. De Schryver, C. Geelen, D. Terrell and S. De Meutter, *Macromolecules*, 1993, **26**, 472–478.

[10] G. Verbeek, A. Vaes, M. Van der Auweraer, F. C. De Schryver, C. Geelen, D. Terrell and S. De Meutter, *Macromolecules*, 1993, **26**, 4074.

[11] S. Bharill, P. Sarkar, J. D. Ballin, I. Gryczynski and G. M. Wilson, *Anal. Biochem.*, 2008, **377**, 141–149.

[12] D. R. James and W. R. Ware, *Chem. Phys. Lett.*, 1986, **126**, 7–11.

[13] A. K. Livesey and J. C. Brochon, *Biophys. J.*, 1987, **52**, 693–706.

[14] A. Siemiarczuk, B. D. Wagner and W. R. Ware, *J. Phys. Chem.*, 1990, **94**, 1661–1666.

[15] M. Abramowitz and I. A. Stegun, *Handbook of Mathematical Functions*, Dover Publications, Inc., New York, 1965.

[16] R. K. Neely, D. Daujotyte, S. Grazulis, S. W. Magennis, D. T. F. Dryden, S. Klimašauskas and A. C. Jones, *Nucleic Acids Res.*, 2005, **33**, 6953–6960.

[17] T. M. Nordlund, S. Andersson, L. Nilsson, R. Rigler, A. Gräslund and L. W. McLaughlin, *Biochemistry*, 1989, **28**, 9095–9103.

[18] R. A. Hochstrasser, T. E. Carver, L. C. Sowers and D. P. Millar, *Biochemistry*, 1994, **33**, 11971–11979.

[19] T. Lenz, E. Y. M. Bonnist, G. Pljevaljčić, R. K. Neely, D. T. F. Dryden, A. J. Scheidig, A. C. Jones and E. Weinhold, *J. Am. Chem. Soc.*, 2007, **129**, 6240–6248..

[20] K. D. Raney, L. C. Sowers, D. P. Millar and S. J. Benkovic, *Proc. Natl. Acad. Sci. U. S. A.*, 1994, **91**, 6644–6648.

[21] M. Menger, T. Tuschl, F. Eckstein and D. Porschke, *Biochemistry*, 1996, **35**, 14710–14716.

[22] J. M. Beechem, M. R. Otto, L. B. Bloom, R. Eritja, L. J. Reha-Krantz and M. F. Goodman, *Biochemistry*, 1998, **37**, 10144–10155.

[23] W. R. Ware, L. J. Doemeny and T. L. Nemzek, *J. Phys. Chem.*, 1973, **77**, 2038–2048.

[24] A. E. McKinnon, A. G. Szabo and D. R. Miller, *J. Phys. Chem.*, 1977, **81**, 1564–1570.

[25] W. H. Press, B. P. Flannery, S. A. Teukolsky and W. T. Vetterling, *Numerical Recipes in FORTRAN 77: The Art of Scientific Computing*, Cambridge University Press, Cambridge, 2nd edn, 1993.

[26] R. Luchowski, Z. Gryczynski, P. Sarkar, J. Borejdo, M. Szabelski, P. Kapusta and I. Gryczynski, *Rev. Sci. Instrum.*, 2009, **80**, 033109.

[27] J. Večeř, A. A. Kowalczyk and R. E. Dale, *Rev. Sci. Instrum.*, 1993, **64**, 3403–3412.

[28] J. Večeř, A. A. Kowalczyk, L. Davenport and R. E. Dale, *Rev. Sci. Instrum.*, 1993, **64**, 3413–3424.

[29] K. Binder and D. P. Landau, *A Guide to Monte Carlo Simulations in Statistical Physics*, Cambridge University Press, Cambridge, 2nd edn, 2005.

[30] M. Lee, J. Tang and R. Hochstrasser, *Chem. Phys. Lett.*, 2001, **344**, 501–508.

[31] V. Z. Marmarelis, *Ann. Biomed. Eng.*, 1993, **21**, 573–589.

[32] J.-M. I. Maarek, L. Marcu, W. J. Snyder and W. S. Grundfest, *Photochem. Photobiol.*, 2000, **71**, 178–187.

[33] FAST Data Acquisition and Analysis Software, Edinburgh Instruments, Livingston EH54 7DQ, UK.

[34] D. Magde, G. E. Rojas and P. G. Seybold, *Photochem. Photobiol.*, 1999, **70**, 737–744.

[35] D. Magde, R. Wong and P. G. Seybold, *Photochem. Photobiol.*, 2002, **75**, 327–334.

[36] R. K. Neely and A. C. Jones, *J. Am. Chem. Soc.*, 2006, **128**, 15952–15953.

[37] M. A. O'Neill and J. K. Barton, *J. Am. Chem. Soc.*, 2004, **126**, 11471–11483.

[38] M. A. O'Neill and J. K. Barton, *J. Am. Chem. Soc.*, 2004, **126**, 13234–13235.

[39] C. R. Guest, R. A. Hochstrasser, L. C. Sowers and D. P. Millar, *Biochemistry*, 1991, **30**, 3271–3279.

[40] E. L. Rachofsky, R. Osman and J. B. A. Ross, *Biochemistry*, 2001, **40**, 946–956.

[41] J. R. Lakowicz, *Principles of Fluorescence Spectroscopy*, Springer, New York, 3rd edn, 2006.

[42] O. J. Rolinski and D. J. S. Birch, *J. Chem. Phys.*, 2000, **112**, 8923–8933.

[43] O. J. Rolinski, D. J. S. Birch, L. J. McCartney and J. C. Pickup, *Chem. Phys. Lett.*, 2000, **324**, 95–100.